The role and analysis of molecular systems in electrocatalysis

Dijk, B. van

Chapter 5

Mechanistic insight from structure–activity studies in the electrochemical oxygen reduction by substituted tris(2-pyridylmethyl)amine copper complexes

*Structural modifications in the ligand system of molecular complexes can lead to improvement of activity and reduce the overpotential for electrochemical reactions. Many copper complexes with diverse structural differences have been reported for the O_2 reduction reaction, but the influence of electron withdrawing substituents had not yet been clearly investigated by a structure–activity study. To contribute to this field, we have investigated the effect of NH_2 (**3**^{NH2}), Cl (**2**^{Cl}), and CF_3 (**2**^{CF3}) as substituents on the oxygen reduction activity of the tris(2-pyridylmethyl)amine copper complex (**1**); a recently reported very fast molecular copper complex for the oxygen reduction reaction. We found that the redox couple, as expected, had a clear correlation between the Hammett parameters of the substituents and the $E_{1/2}$ of the redox couple. On the other hand, the onset for O_2 reduction was not affected by the substituents as was determined with rotating ring disk electrode (RRDE) experiments. Non-rotating electrode experiments and a Tafel analysis derived from the RRDE data indicated that only **2**^{Cl} had a higher rate for O_2 reduction with respect to **1**. In contrast, **2**^{CF3} did not have improved reactivity and **3**^{NH2} displayed significantly lower reactivity than **1**. On the other hand, the electron withdrawing effect of **2**^{Cl} and **2**^{CF3} shifted the onset potential for H_2O_2 reduction 150 mV positive with respect to **1**. Moreover, the rate had increased with respect to **1**. The remarkable results of O_2 reduction has led to a new insight in the O_2 reduction mechanism, wherein we propose that a Cu^{II} to Cu^{II}–$O_2^{\bullet-}$ step is the observed potential determining step instead of the $Cu^{I/II}$ redox couple of the complex because the rate of O_2 reduction is very fast compared to the experimental scan rate. The significant outcome is that the onset potential for O_2 reduction cannot be easily adjusted by electronic effects of substituents. On the other hand, we have shown that H_2O_2 reduction is affected by these electronic effects. We found that electron withdrawing groups has a beneficial effect on both the onset potential as well as the catalytic rate.*

The results in this chapter are to be submitted as: B. van Dijk, A. E. Herzog, K. D. Karlin, D. G. H. Hetterscheid, *Mechanistic insight from structure–activity studies in the electrochemical oxygen reduction by substituted tris(2-pyridylmethyl)amine copper complexes*

5.1 Introduction

The electrochemical O_2 reduction reaction is an important and versatile reaction. A major aspect is that two different products can be formed with their own applications and challenges. The 4 electron reduction to H_2O plays a central role in fuel cell chemistry. To electrochemically oxidize (sustainably produced) H_2 for electricity generation, O_2 to H_2O reduction has to take place at the cathode. However, even with the best catalysts to date (Pt-based) there are significant energy losses in the form of 400 mV overpotentials.[1-3] The other possible outcome of O_2 reduction is the 2 electron O_2 to H_2O_2 reduction that is a viable and environmentally friendly alternative for the current anthraquinone process for the production of H_2O_2.[4, 5] The waste generation and energy requirements of the latter process make H_2O_2 one of the most expensive bulk chemicals even though it has diverse (green) applications.[6-9] Obviously, for either goal a highly active and selective catalyst with minimal overpotential would be desired.

Recently, our group has shown that complex **1** (Chart 5.1) displays very high reaction rates for the electrochemical O_2 reduction reaction.[10] It was found that O_2 is reduced in two separate catalytic cycles. In the first cycle, O_2 is reduced to H_2O_2. This cycle was proposed to start with the fast reduction of the complex to Cu^I (Equation 5.1). In the next step, suggested as the rate determining step, the reduced Cu^I complex coordinates O_2 and forms a radical superoxo complex (Equation 5.2). Subsequently, the complex further reduces via a proton coupled electron transfer step to an end-on hydroperoxo complex (Equation 5.3) which will release H_2O_2 after protonation. H_2O_2 was found as a detectable intermediate. In the second cycle, the further two electron reduction of H_2O_2 to H_2O takes place. The difference between the equilibrium potential of the desired reaction and the actual onset potential at which catalysis starts, was still around 0.2 V for O_2 to H_2O_2 reduction. This is not

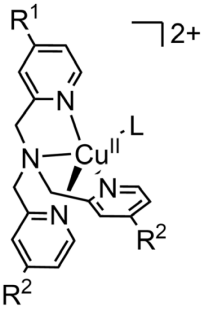

1: $R^1 = H, R^2 = H$
2^{Cl}: $R^1 = Cl, R^2 = Cl$
2^{CF3}: $R^2 = CF_3, R^2 = CF_3$
3^{NO2}: $R^1 = H, R^2 = NO_2$
3^{NH2}: $R^1 = H, R^2 = NH_2$

Chart 5.1. Structure and nomenclature of the copper complexes.

based on the standard equilibrium potential of O_2 to H_2O, which is 1.23 V *versus* RHE (reversible hydrogen electrode), but on the 2 electron O_2 to H_2O_2 equilibrium potential of 0.695 V *versus* RHE.[11] The overall rate of the two catalytic cycles for the total 4 electron reduction of O_2 to H_2O was determined at $1.5 \times 10^5 \pm 0.2 \times 10^5$ s^{-1}. The direct determination of the rate constant was possible with the current enhancement method which uses the peak catalytic current and peak current of the reduction the complex to Cu^I (see Chapter 1).[12] Of note, this rate was determined with very low catalyst concentrations (0.1 – 1.0 μM) since the O_2 solubility in water is around 1.2 mM and this way substrate availability does not influence the observed rate significantly. The rate for the O_2 to H_2O_2 reduction, the first catalytic cycle, was calculated with a foot of the wave analysis (FOWA) which is performed close to the onset of the catalytic current to avoid any side-phenomena (such as substrate depletion) so that the current can be assumed to be purely kinetic in nature.[13-16] Of note, the FOWA does not determine the actual rate of catalysis, but estimates the maximum rate, or the maximum turnover frequency (TOF_{max}). From the FOWA, a TOF_{max} of $1.8 \times 10^6 \pm 0.6 \times 10^6$ s^{-1} was determined which is in close agreement with the overall rate as obtained with the current enhancement method showing that O_2 reduction catalysis at low catalyst concentrations is close to the maximum rate. For the FOWA, an EC mechanism was assumed in which the rate determining, chemical step is Equation 5.2 which is preceded by fast reduction of **1** with the potential determining step being related to the $E_{1/2}$ of the $Cu^{I/II}$ redox couple. The rate constant for Equation 5.2 (k_2) would actually be the same as the rate of O_2 coordination (k_{O2}) to the Cu^I complex. The rate would be linked via $k_2 = [O_2]k_{O2}$. k_{O2} for the Cu^I complex of **1** has previously been determined to be 1.3×10^9 M^{-1} s^{-1} in THF.[17] When correcting for the 1.2 mM O_2 concentration in phosphate buffer, the same order of magnitude (10^6 s^{-1}) as the TOF_{max} is obtained.

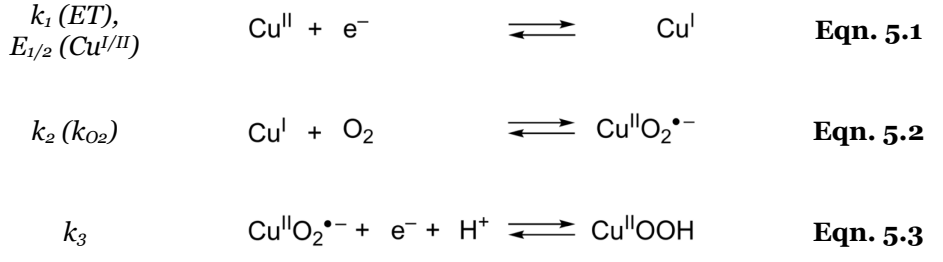

O_2 reduction catalysis by **1** is very fast, but there is still a 0.2 V difference between the equilibrium potential of O_2 to H_2O_2 and the onset potential. Placing substituents on the pyridines of the tmpa ligand (tmpa = tris(2-

pyridylmethyl)amine) of **1** could help to affect the $E_{1/2}$ and the rate of catalysis. A previous study suggested that O_2 coordination to form the end-on superoxo intermediate (Eqn. 5.2) is favored by strong electron donating substituents on the *para* position of the pyridines of the tmpa ligand (tmpa = tris(2-pyridylmethyl)amine) and would thus increase k_1 of Equation 5.2.[18] However, another study reported that electron donating cyclic amine substituents on the tmpa ligand decreased the $E_{1/2}$ and thereby increasing the energy of the HOMO.[19] The latter was found to increase the rate of atom transfer radical polymerization reactions by facilitating the formation of Cu–X species (X = halogen). Interestingly, one studied claimed that NH_2 in the *ortho* position did not affect the onset nor the Tafel slope of O_2 reduction with respect to **1**.[20] This remarkable result was explained as that not the $Cu^{I/II}$, nor a protonation step would be rate determining, but the O–O bond cleavage step would be. However, this specific electrocatalytic study was performed at pH 1. At this pH, the pyridines are protonated at the nitrogen and are unable to coordinate to copper.[21] Essentially, the molecular complexes cannot exist under the experimental conditions. Since the other studies did suggest that substitution of **1** (or related complexes) affects the catalytic activity and the $E_{1/2}$, we placed NO_2, NH_2 , CF_3, and Cl[19] substituents on the *para* positions of the pyridines of **1** (Chart 5.1) to understand if and how substituents could improve the rate of electrocatalytic O_2 and H_2O_2 reduction and the onset potential.

5.2 Results

5.2.1 Strategy and synthesis of $\mathbf{3^{NO2}}$ and $\mathbf{3^{NH2}}$

Placing electron donating (EDG) or withdrawing groups (EWG) on the ligand framework was expected to electronically steer the reaction rate and/or selectivity. Especially aromatic (heterocyclic) rings allow for the precise position of both electron withdrawing or donating groups. Louis Hammett found that these substituents could be described by a parameter (σ) and linked to properties such as the pK_a of benzoic acids and phenols, the rate of esterification or hydrolysis of aromatic compounds, or the rate of bromination of acetophenone.[22, 23] Based on these Hammett parameters, specific substituents can be chosen to apply the withdrawing or donating effect to a complex and its reactivity in catalysis. The $E_{1/2}$ of the $Cu^{I/II}$ redox couple of the complexes can be shifted depending on the electronic nature of the substituents. Less electron density around the metal center, induced by EWG, will shift the $Cu^{I/II}$ redox couple to higher potentials while an EDG will lower the $E_{1/2}$. We set out to investigate EWG's on the ligand framework of **1** as we expect

these to shift the $E_{1/2}$ of the $Cu^{I/II}$ redox couple to higher potentials which is proposed as the potential determining step for O_2 to H_2O_2 reduction (Eqn. 5.1). In that retrospect, we were interested in studying the effect of Cl, CF_3, and NO_2 substituents that have Hammett parameters of 0.23, 0.54, and 0.78, respectively for the *para* position. Complexes $\mathbf{2^{Cl}}$ and $\mathbf{2^{CF3}}$ have all three pyridines substituted at the *para* position and were obtained from the laboratory of K. D. Karlin at the John Hopkins University. Likewise, we were interested in synthesizing the NO_2 analogue. As this analogue could be easily converted to the NH_2 analogue by reduction, we also synthesized the NH_2 analogue for comparison since it has a lower (-0.66) Hammett parameter than tmpa (0 by definition).

For the synthesis of a ligand with three pyridines substituted with NH_2 at the *para* position, 2-aminomethyl-4-nitro-pyridine is required as an intermediate. Compound **5** (Scheme 5.1) is the starting material for 2-aminomethyl-4-nitropyridine, but also required for the S_N2 reaction with an amine to obtain the desired tripodal ligand. However, compound **5** was found to be highly unstable in the solid state and was thus immediately used further in the synthesis after purification to minimize the loss in yield. For that reason, 2-aminomethylpyridine instead of 2-aminomethyl-4-nitropyridine was used which resulted in ligand **6** with two instead of three substituted pyridines via an S_N2 reaction. To obtain the unstable intermediate **5**, compound **4** was prepared by the reaction of the commercially available 4-nitro-2-picoline-N-oxide with trifluoroacetic anhydride and subsequent hydrolysis. The hydroxymethyl-pyridine **4** was then converted into the

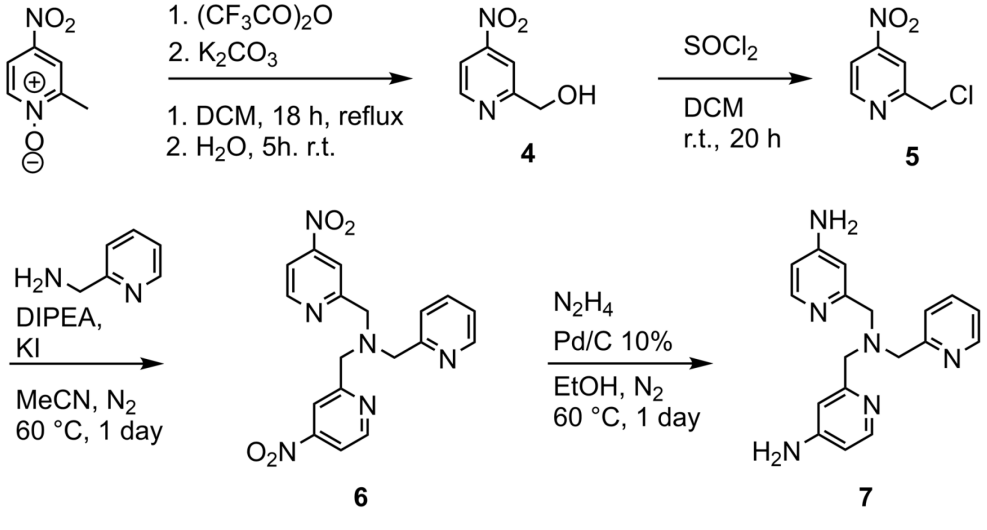

Scheme 5.1. Synthetic route to the ligands **6** and **7**.

chloromethyl-pyridine **5**. Ligand **6** was characterized by ^{1}H nuclear magnetic resonance (NMR), ^{13}C NMR and high resolution mass spectroscopy (HR MS). The NH_2 analogue, ligand **7**, was prepared from **6** by catalytic reduction of the nitro groups with Pd/C and hydrazine as reducing agent. **7** was characterized by NMR and MS as well. Next the corresponding copper complexes $\mathbf{3}^{\mathbf{NO_2}}$ and $\mathbf{3}^{\mathbf{NH_2}}$ were synthesized. $\mathbf{3}^{\mathbf{NO_2}}$ was synthesized by mixing $Cu(OTf)_2$ (OTf = $CF_3SO_3^-$) and **6** in methanol. The complex was crystallized to produce blue crystals by vapor diffusion of diethyl ether (Et_2O) into acetonitrile (MeCN). Unfortunately, no suitable crystals for structure determination by X-Ray diffraction were obtained. Elemental analysis confirmed that [Cu(**6**)(MeCN)]$(OTf)_2$ was obtained in purified form. The NO_2 groups of $\mathbf{3}^{\mathbf{NO_2}}$ were found to electrochemically reduce in the same potential window as where the redox couple and any O_2/H_2O_2 reduction activity would be expected (Figure D.1). Therefore, this complex was not further studied. The complex $\mathbf{3}^{\mathbf{NH_2}}$ was synthesized in the same way by mixing **7** and $Cu(OTf)_2$. However, $\mathbf{3}^{\mathbf{NH_2}}$ could not be crystallized into a solid form. Probably, hydrogen bonding of the amine with water hinders crystallization. The ligand only dissolves in water and MeOH which limited further crystallization possibilities. When $Cu(OTf)_2$ and **7** are mixed in water (or methanol), the solution turns immediately green in color. This indicates that the complex is formed instantaneous and is characterized by absorptions at 260 nm, 270 nm, *circa* 300 nm (broad), and low intensity, broad absorptions at 700 and 900 nm in the UV-vis spectrum (Figure D.2). Therefore, measurements were performed with the *in situ* formed complex by mixing $Cu(OTf)_2$ and **7** in water in a 1 : 1 ratio and subsequently mixing it with phosphate buffer. Of note, minor impurities are likely still present since purification was not possible which could lead to deposits. Nevertheless, the complex shows a clear redox couple and its cyclic voltammogram (CV) of O_2 and H_2O_2 reduction activity can be compared.

5.2.1 Electrochemistry of $\mathbf{2}^{\mathbf{Cl}}$, $\mathbf{2}^{\mathbf{CF_3}}$, and $\mathbf{3}^{\mathbf{NH_2}}$

To study the substituent effect on the redox couple, cyclic voltammograms of the complexes in pH 7 phosphate buffer under argon atmosphere were recorded (Figure 5.1). In addition, cyclic voltammograms at 100 mV/s scan rate of **1**, $\mathbf{2}^{\mathbf{Cl}}$, $\mathbf{2}^{\mathbf{CF_3}}$, and $\mathbf{3}^{\mathbf{NH_2}}$ are overlaid in Figure 5.1D. As mentioned before, no data for $\mathbf{3}^{\mathbf{NO_2}}$ could be acquired since the NO_2 groups are electrochemically reduced in this potential window (Figure D.1). At first sight, the peak current of the substituted complexes is lower than that of **1**. This is caused by lower diffusion coefficients of these complexes as compared to **1** which were determined using the Randles–Sevcik equation (see

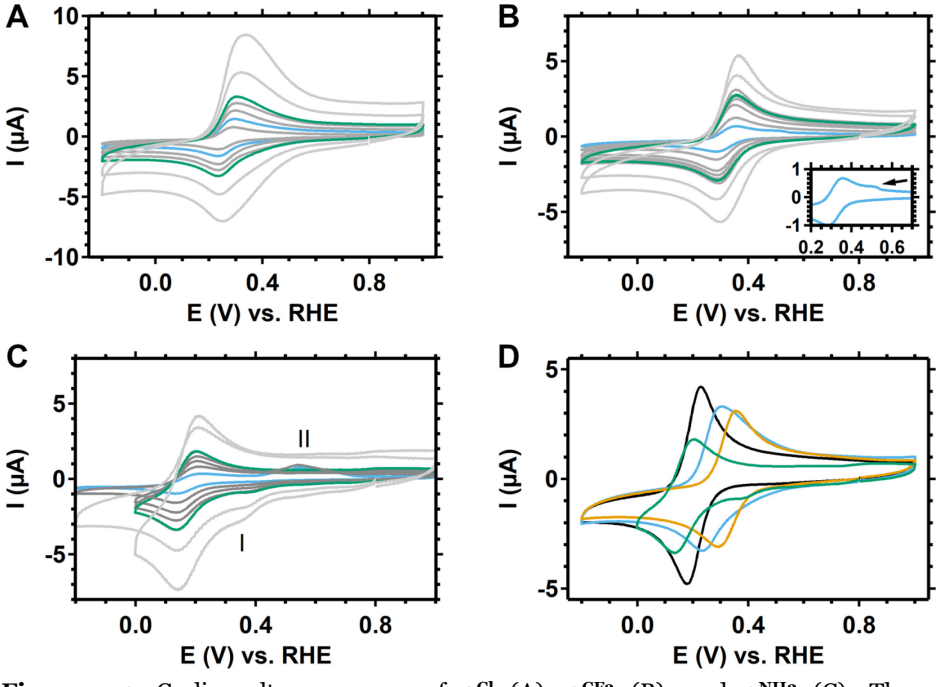

Figure 5.1. Cyclic voltammograms of $\mathbf{2}^{Cl}$ (A), $\mathbf{2}^{CF_3}$ (B), and $\mathbf{3}^{NH_2}$ (C). The cyclic voltammograms were recorded at scan rates from 25 mV/s (blue) to 100 mV/s (green) in argon purged 0.1 M phosphate buffer of pH 7. Scan rates of 200 and 400 mV/s are depicted in light grey. Catalyst concentration was 0.3 mM. (D) shows $\mathbf{2}^{Cl}$ (blue), $\mathbf{2}^{CF_3}$ (orange), and $\mathbf{3}^{NH_2}$ (green) with **1** (black) at 100 mV/s. Data of **1** was adapted from reference 10.

Chapter 1).[16] The diffusion coefficients for $\mathbf{2}^{Cl}$ (2.0×10^{-6} cm²/s), $\mathbf{2}^{CF_3}$ (1.8×10^{-6} cm²/s), and $\mathbf{3}^{NH_2}$ (1.3×10^{-6} cm²/s) are less than half of that of **1** (4.9×10^{-6} cm²/s).[10]

The electron withdrawing or donating capabilities of the substituted complexes **2** and **3** can be best described by the σ_p as Hammett parameter for substituents on the *para* position. As expected, the EWG's of $\mathbf{2}^{Cl}$ and $\mathbf{2}^{CF_3}$ shift the $E_{1/2}$ of the redox couple to higher potentials with respect to **1**. Specifically, the $E_{1/2}$ of the complexes shifts from 0.21 V (**1**) to 0.27 V ($\mathbf{2}^{Cl}$) and 0.32 V ($\mathbf{2}^{CF_3}$). On the other hand, the $E_{1/2}$ of $\mathbf{3}^{NH_2}$ is lower than **1** at 0.17 V due to the electron donating character of NH_2. The $E_{1/2}$ values of the complexes are plotted *versus* the σ_p of the substituents in Figure 5.2A. There is a clear correlation even though the fit is not perfect. Given that the complexes have either 2 or 3 substituted pyridines, Figure 5.2B was constructed where the σ_p of $\mathbf{3}^{NH_2}$ was normalized by the number of substituents introduced at the ligand. This normalization of the Hammett parameter gave a better linear fit (Figure 5.2B) which is illustrated by a higher R^2 value.

The peak separation between the reduction and oxidation peaks provides information about the (ir)reversibility of the redox couple. The cyclic voltammogram of $\mathbf{2}^{\mathbf{Cl}}$ at scan rates above 100 mV/s appear to be less reversible since both the reductive and oxidative peaks broaden (Figure 5.1A). At those high scan rates, there may be some underlying equilibrium that becomes visible. The electron withdrawing character of the chloride groups might elongate the Cu–N bond of the pyridines. It could be that one, or more of these Cu–N bonds are replaced with H_2O or phosphate in a dynamic equilibrium. However, no second redox couple was found at lower scan rates which would be indicative of the presence of more than one species. A second oxidation did appear at low scan rates in the cyclic voltammogram of $\mathbf{2}^{\mathbf{CF3}}$. In general, the oxidation peak is relatively broad and a second oxidation was observed at 0.52 V at a scan rate of 10 mV/s (Figure 5.1B). No second reduction peak is observed indicating that this second oxidation seems to belong to a species that is formed during the reduction of $\mathbf{2}^{\mathbf{CF3}}$. The cyclic voltammogram of $\mathbf{3}^{\mathbf{NH2}}$ has some oxidative peaks that arise from the minor impurities which are indicated by II in Figure 5.1C. These oxidations were not visible when the lower potential limit was set at 0.0 V instead of –0.2V and are possibly related to Cu^0 deposition. In addition, a reductive peak was observed as indicated by I in Figure 5.1C. This reduction relates to the reduction of a small remnant of O_2. Normally, the second scan can be used in that case since all the O_2 has reduced away by the time the second scan starts. However, small impurities in a solution containing $\mathbf{3}^{\mathbf{NH2}}$ can electrodeposit on the electrode and thereby influence the cyclic voltammogram significantly in the second scan. Thus, the first scan was used for $\mathbf{3}^{\mathbf{NH2}}$. Interestingly, Laviron plots of the potential of the oxidative and reductive peaks of the complexes *versus* the scan rate show that the peak positions do not shift up to 100 mV/s (Figure D.4) and the peak separation does not widen above 100 mV/s. An increase in peak separation could indicate a

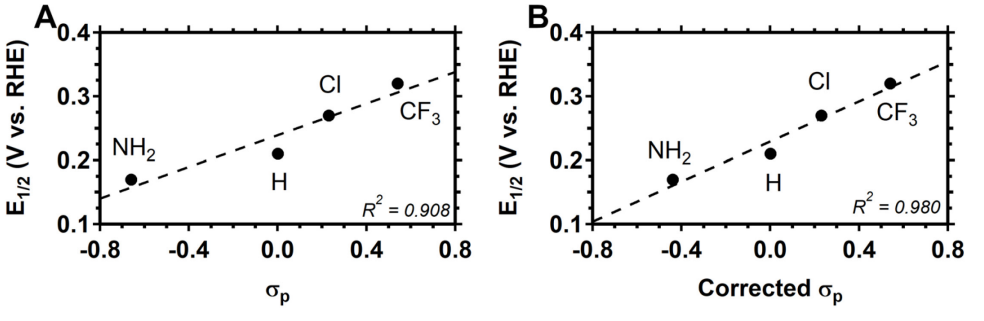

Figure 5.2. Correlation of the Hammett parameter of the substituents and the $E_{1/2}$ of the corresponding complexes. Dashed lines are linear fits. For B, the σ_p of NH_2 was multiplied by 0.667 (2/3).

slower electron transfer,[24] thus it seems that electron transfer for $\mathbf{2}^{Cl}$, $\mathbf{2}^{CF_3}$, and $\mathbf{3}^{NH_2}$ is still fast in contrast to other related complexes such as the dinuclear copper complex described in Chapter 4 and mononuclear copper complex with terpyridine and 2,2'-dimethylpyridylamine ligands.[24]

The magnitude of the peak current varies with the scan rate. As can be derived from the Randles-Sevcik equation (Chapter 1), a linear relationship between the square root of the scan rate and the peak current indicates that diffusive processes play a role for the observed species. Otherwise, there is a direct linear relationship with the peak current. For complexes $\mathbf{2}^{Cl}$, $\mathbf{2}^{CF_3}$, and $\mathbf{3}^{NH_2}$, the best fit is obtained when the peak current is plotted *versus* the square root of the scan rate rather than directly *versus* the scan rate (Figure 5.3). The fits of $\mathbf{3}^{NH_2}$ are of less quality, but for this complex the data fits best when the square root of the scan rate is considered. Therefore, diffusive processes play a role for the (major) redox feature, which belong to the redox couple of the complexes. Following, the complexes themselves are most likely homogeneous in nature.

5.2.2 O_2 and H_2O_2 reduction with non-rotating electrodes

Compound **1** reduces O_2 in a stepwise mechanism wherein H_2O_2 is formed as detectable intermediate before it is further reduced to H_2O. Therefore, both O_2 and H_2O_2 reduction were addressed separately (Figure 5.4). First of all, O_2 reduction is

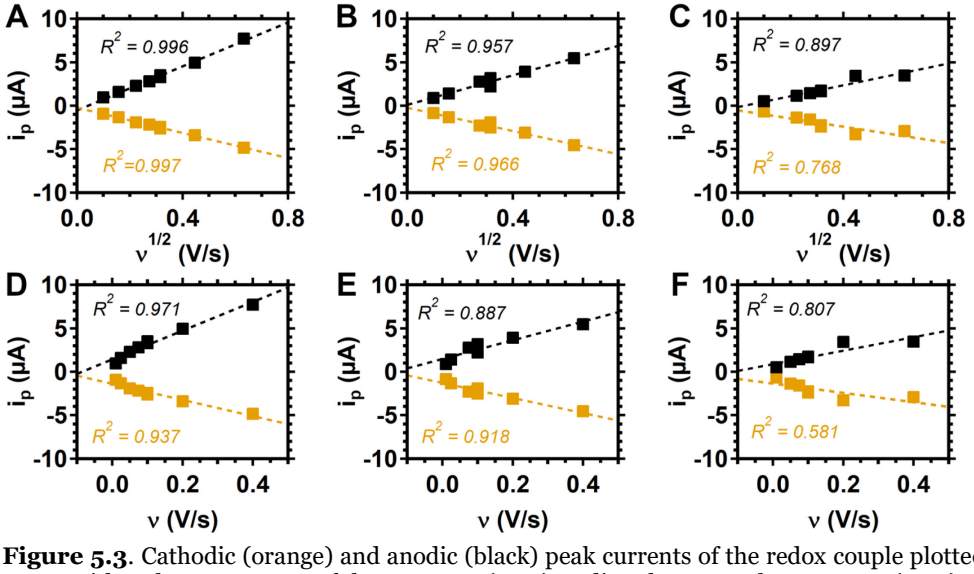

Figure 5.3. Cathodic (orange) and anodic (black) peak currents of the redox couple plotted *versus* either the square root of the scan rate (A–C) or directly *versus* the scan rate (D–F) of the complexes $\mathbf{2}^{Cl}$ (A and D), $\mathbf{2}^{CF_3}$ (B and E), and $\mathbf{3}^{NH_2}$ (C and F). Dashed lines are linear fits.

considered. Differences in onset potential and peak potential of O_2 reduction by the complexes are visible from the overlay of the voltammograms of complexes **1**, $\mathbf{2}^{Cl}$, $\mathbf{2}^{CF3}$, and $\mathbf{3}^{NH2}$ in Figure 5.4. At first sight, the current of **1** and $\mathbf{2}^{Cl}$ overlap near the onset of O_2 reduction. The same applies to the onset potential for $\mathbf{2}^{CF3}$ and $\mathbf{3}^{NH2}$, but these complexes start reducing O_2 around 50 mV lower. Of note, there is a large experimental error up to 75 mV in the apparent onset potential (Figure D.5). In the next section, the use of rotating electrodes is described whereby the experimental error was smaller and the onset potential is more accurate. The displayed CV's in Figure 5.4 also render information regarding the rate of catalysis. A larger catalytic rate results in higher currents, thus a steeper slope of would indicate faster catalysis.[13] In that sense, $\mathbf{2}^{Cl}$ (and to a lesser extent $\mathbf{2}^{CF3}$ as well) seems to catalyze the reduction of O_2 with a higher rate because the reductive current has a steeper slope than **1**. Beware that the catalytic current of the cyclic voltammogram encompasses both O_2 to H_2O_2 and H_2O_2 to H_2O reduction and catalysis is significantly hindered since the O_2 concentration is just one order of magnitude higher than the catalyst concentrations (1.2 mM *versus* 0.3 mM). The lower catalytic rate of $\mathbf{3}^{NH2}$ is more evident from the CV as its slope is less steep. In addition, a kink can be seen in the reductive current in the presence of O_2 (Figure 5.4 A). This feature could indicate that apart from O_2 reduction, a second reductive process such as catalyst reduction takes at a higher potential than O_2 reduction.

As opposed to the apparent same onset potential for O_2 reduction, H_2O_2 reduction by $\mathbf{2}^{Cl}$ starts at a 200 mV higher potential than **1**. The other complex bearing an EWG ($\mathbf{2}^{CF3}$) has a positive shift in H_2O_2 reduction as well, albeit around 100 mV with respect to **1**. The current profile between the onset and the peak

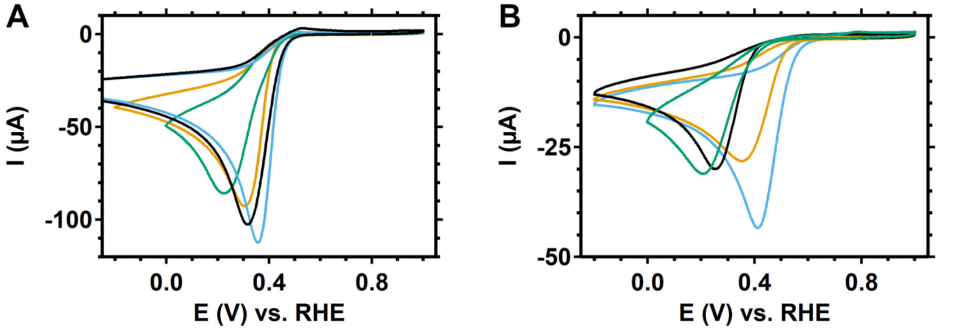

Figure 5.4. Cyclic voltammograms of O_2 reduction (A) and H_2O_2 reduction (B) by 0.3 mM **1** (black), $\mathbf{2}^{Cl}$ (blue), $\mathbf{2}^{CF3}$ (orange), and $\mathbf{3}^{NH2}$ (green). The CV's were recorded at 100 mV/s in 0.1 M phosphate buffer of pH 7 that was either saturated with 1 atm O_2 (A) or argon (B). 1.1 mM H_2O_2 was added to the solution for B. Data of **1** was adapted from reference 10.

catalytic current is considerably steeper in the case of $\mathbf{2}^{\mathbf{Cl}}$ than in the case of $\mathbf{2}^{\mathbf{CF3}}$ and **1** pointing to faster catalysis. Complex $\mathbf{3}^{\mathbf{NH2}}$ with an EDG starts H_2O_2 reduction at the same potential as **1** within the experimental error range. Clearly, the slope of the current is less steep, signifying slower catalysis than **1**. The presence of a second reductive process, as was the case for O_2 reduction, is not clear from the voltammogram, even though the onset potential is around 0.4 V for both O_2 and H_2O_2 reduction.

In general, the onset for O_2 reduction does not change significantly based on the EWG or EDG and is actually within the experimental error. The voltammogram of $\mathbf{2}^{\mathbf{Cl}}$ does suggest faster catalysis (overall for the O_2 to H_2O reduction) than **1**. For the H_2O_2 to H_2O reduction, the differences in onset potential are larger and outside the range of the experimental error. H_2O_2 reduction clearly starts at a higher potential for both $\mathbf{2}^{\mathbf{Cl}}$ and $\mathbf{2}^{\mathbf{CF3}}$ with EWG's with respect to the unsubstituted complex **1**. Moreover, the voltammogram of $\mathbf{2}^{\mathbf{Cl}}$ suggests faster catalysis. Interestingly, the Hammett parameter for $\mathbf{2}^{\mathbf{Cl}}$ is lower than for $\mathbf{2}^{\mathbf{CF3}}$ which might suggest that not only the electron withdrawing character of the chloride group influence the reactivity. In all cases, the onset potential of $\mathbf{3}^{\mathbf{NH2}}$ does not significantly differ from **1** and the voltammogram indicates that both O_2 and H_2O_2 reduction is more sluggish.

5.2.3 O_2 and H_2O_2 reduction with rotating (ring) disk electrode

As introduced in Chapter 1, the rotating ring disk electrode (RRDE) is an experimental setup that controls diffusion. Due to the creation of a laminar flow of electrolyte towards the electrode, the diffusion is constant and no longer dependent on the scan rate.[25] This way, the catalytic onset potential can be more accurately compared as the influence of experimental errors could be diminished (Figure D.6). Moreover, the ring electrode around the GC work electrode can be put to use as an electrochemical sensor for H_2O_2 by constantly applying a potential of 1.2 V. O_2 and H_2O_2 reduction were therefore studied by RRDE in a pH 7 phosphate buffer at 1600 rpm electrode rotation rate.

Whereas the results of the non-rotating electrode experiments showed differences in onset potential, the RRDE measurements clearly indicate that these differences should be ascribed to the experimental error. As seen in Figure 5.5A (and the zoom), complexes **1** and $\mathbf{2}^{\mathbf{CF3}}$ have the same onset potential. $\mathbf{2}^{\mathbf{Cl}}$ seem to start reducing O_2 at a 50 mV lower potential, but again this is within the experimental error limit (Figure D.6). Moreover, the current profiles of **1** and $\mathbf{2}^{\mathbf{Cl}}$ overlap almost perfectly. Initially, $\mathbf{2}^{\mathbf{CF3}}$ follows the same profile, but deviates at lower potential because a lower diffusion limited current is reached. The catalytic performance of

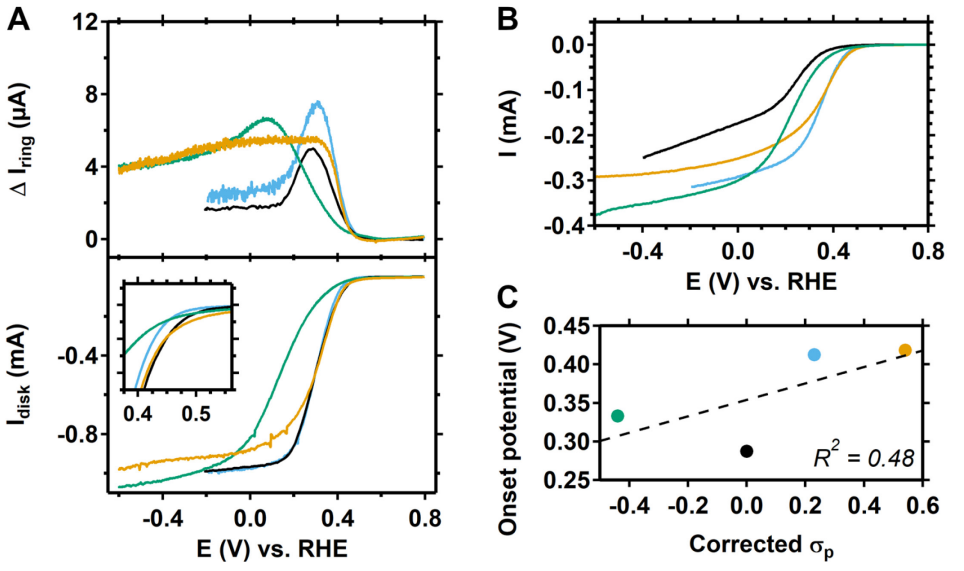

Figure 5.5. Linear sweep voltammograms of O_2 reduction (A, bottom panel) and H_2O_2 reduction (B) by $\mathbf{2}^{Cl}$ (blue), $\mathbf{2}^{CF3}$ (orange), $\mathbf{3}^{NH2}$ (green) and **1** (black), and the onset of H_2O_2 reduction (C, defined as potential where current has reached −50 μA). The Pt ring current (at 1.2 V) is shown in the top panel of A. Scans were recorded at 50 mV/s in a O_2 (A) or Ar (B) saturated 0.1 M phosphate buffer at 0.3 mM catalyst concentration. For B, 1.0 mM H_2O_2 was used. The electrode was rotated at 1600 rpm. Data of **1** was adapted from reference 10.

$\mathbf{3}^{NH2}$ is clearly less than that of the other complexes since it only reaches the diffusion limited current at −0.2 V whereas the other complexes do so around 0.2 V. In the potential window between the onset and the diffusion limited current, the ring current indicates that H_2O_2 is partially produced in the case of all complexes. For **1** and $\mathbf{2}^{Cl}$, a maximum ring current is reached before it levels off.

The maximum ring current differs for **1** and $\mathbf{2}^{Cl}$, but can be explained by the difference in collection efficiency for H_2O_2 of the ring (12.5% for $\mathbf{1}$[10] and pre-determined at 14.8% for $\mathbf{2}^{Cl}$). As explained in Appendix C, the collection efficiency of the Pt ring for H_2O_2 can be best pre-determined for every experiment to have a reliable collection efficiency. Following, the collection efficiency was determined prior to the measurement of $\mathbf{2}^{Cl}$ by a 3 minute amperogram at −0.1 V disk potential in catalyst-free electrolyte. As the current profiles on the disk overlap for **1** and $\mathbf{2}^{Cl}$, it is not expected that there is a difference in H_2O_2 selectivity. On the other hand, the ring current profile of $\mathbf{2}^{CF3}$ indicates that H_2O_2 is produced in significant quantities even when the diffusion limited current is reached. In detail, in the potential window between 0.0 and −0.2 V, the average ring current was 5.5 μA where the disk current was 800 μA . Together with a pre-determined collection efficiency of 10.2% prior to

the measurement of $\mathbf{2}^{\mathbf{CF_3}}$, the percentage of H_2O_2 was calculated using Eqn. C.1 to be 12.5%.This also explains why the magnitude of the disk current of $\mathbf{2}^{\mathbf{CF_3}}$ is less than for **1** and $\mathbf{2}^{\mathbf{Cl}}$. A higher selectivity for H_2O_2 inherently results in less electrons that have to be transferred (2 electron *versus* 4 electron reduction of O_2). $\mathbf{3}^{\mathbf{NH_2}}$ also produces significantly more H_2O_2. Moreover, the diffusion limited current is not reached before the potential limit (<0.0V) where electrodeposition starts to play a role as well (Figure D.3). Also, a new feature is observed on the ring current after prolonged scanning (Figure D.3). Thus, a reliable percentage of H_2O_2 cannot be determined. Nevertheless, it is expected that the selectivity for H_2O_2 is higher than for $\mathbf{2}^{\mathbf{CF_3}}$ since the ring current is higher and the disk current lower at a potential of 0.0 V for $\mathbf{3}^{\mathbf{NH_2}}$.

The current from the RRDE setup is composed of the diffusion limited current I_L and a kinetic current I_k according to the Koutecký-Levich equation (Eqn. 1.6, Chapter 1). As explained in the introduction, the kinetic current is the theoretical current in absence of any mass transport limitations. Since the diffusion limited current is known, I_k can be calculated. When the potential (or overpotential) is plotted *versus* the logarithm of I_k (or the current density) the Tafel plot is obtained.[25] The linear part of this plot can be fitted to obtain the Tafel slope that bears, in theory, information about the mechanism and catalyst performance. Of note, the Tafel plot and slope are usually applied for catalytic reactions that occur at the surface of a heterogeneous electrocatalyst. Since the electrocatalysts in this case (the complexes) are diffusive species as well, any insight from such a Tafel plot should be taken with care. The constructed Tafel plots for O_2 reduction and corresponding slopes for **1**, $\mathbf{2}^{\mathbf{Cl}}$, $\mathbf{2}^{\mathbf{CF_3}}$, and $\mathbf{3}^{\mathbf{NH_2}}$ are depicted in Figure 5.6A. The kinetic currents of all three complexes lie close together. The slopes of the fits of $\mathbf{2}^{\mathbf{CF_3}}$ and **1** can be considered equal as there is merely a 4 mV/dec difference. The slope of $\mathbf{2}^{\mathbf{Cl}}$ is substantially lower at 70 mV/dec which is indicative of faster catalysis. In addition, the slope of $\mathbf{3}^{\mathbf{NH_2}}$ is substantially higher than the other complexes representing that O_2 catalysis is significantly slower. The Tafel analysis thus supports the visual interpretation of catalytic rates from the non-rotating electrode data for O_2 reduction. In addition, there is no clear correlation to the Hammett parameter (Figure 5.6C). Instead, the data suggests that there is an optimum in reactivity for $\mathbf{2}^{\mathbf{Cl}}$.

Very similar to the non-rotating electrode experiments, there is a large difference in H_2O_2 reduction performance between the complexes bearing EWG's ($\mathbf{2}^{\mathbf{Cl}}$ and $\mathbf{2}^{\mathbf{CF_3}}$) and unsubstituted **1** (Figure 5.5B). The onset potential for H_2O_2 reduction, here defined as the potential at which –50 μA is reached, is plotted *versus* the Hammett parameter of the complexes in Figure 5.5C. There is a positive onset

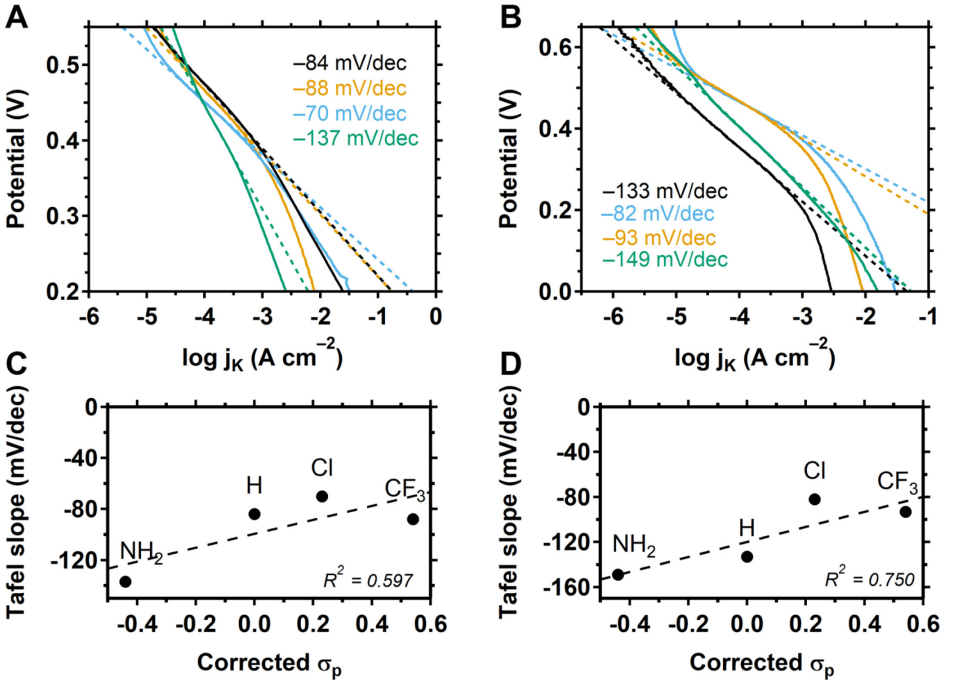

Figure 5.6. Tafel plots of O_2 reduction (A) and H_2O_2 reduction (B) by **1** (black), $\mathbf{2}^{Cl}$ (blue), $\mathbf{2}^{CF3}$ (orange), and $\mathbf{3}^{NH2}$ (green) and the correlation to the Hammett parameter for O_2 (C) and H_2O_2 (D) reduction. The data were obtained in O_2 (A) or argon (B) purged 0.1 M phosphate buffer of pH 7 with 0.3 mM catalyst concentration. The electrode was rotated at 1600 rpm and a scan rate of 50 mV/s was used. 1.0 mM H_2O_2 was used for B. The dashed lines are fits of the linear part of the Tafel plot in A and B. The numbers are the corresponding slopes. Data of **1** was adapted from reference 10.

shift up to 150 mV induced by the EWG's. Interestingly, the onset potential of $\mathbf{3}^{NH2}$ is slightly above that of **1** as well. The Tafel plot of H_2O_2 reduction (Figure 5.6B) emphasizes the large increase in performance due EWG's (Figure 5.6D). Clearly, $\mathbf{2}^{Cl}$ and $\mathbf{2}^{CF3}$ outperform **1** as higher currents at higher potentials are obtained and the respective slopes are significantly lower. For H_2O_2 reduction, the Hammett parameter has a clearer correlation with the catalytic rate (Figure 5.6D) as compared to the results of O_2 reduction, although maximum activity is found for $\mathbf{2}^{Cl}$ as well. Another similarity is that the performance of $\mathbf{3}^{NH2}$ is the lowest of all complexes, but the performance of **1** is just slightly higher for H_2O_2 reduction as opposed to the large difference in O_2 reduction activity between **1** and $\mathbf{3}^{NH2}$. It has to be noted that no real diffusion limited currents for H_2O_2 reduction are reached in the measured potential window. The exact origin is not known, but substrate/product inhibition or catalyst degradation might be taking place simultaneously. A possibility could be that highly reactive radical species, formed in a Fenton type H_2O_2 reduction mechanism, result

in catalyst degradation whereby the conditions for current purely determined by mass transport limitations are not fulfilled.

The RRDE measurements have shown that there are no significant shifts in onset potential for O_2 reduction with EWG's, whereas the onset did shift positively for H_2O_2 reduction. In addition, the Tafel analysis confirms the observations under non-rotating conditions particularly that $\mathbf{2^{Cl}}$ seems to outperform **1** in both O_2 and H_2O_2 reduction whereas $\mathbf{2^{CF3}}$ only shows improved H_2O_2 reduction activity. Interestingly, the H_2O_2 selectivity of $\mathbf{2^{CF3}}$ is higher than the other complexes which is counterintuitive. The lower diffusion limited current in O_2 reduction also points to the fact that not all H_2O_2 that is formed, is further reduced to H_2O by $\mathbf{2^{CF3}}$. As the Tafel analysis indicates that the performance close to the onset for H_2O_2 is intrinsically better than **1**, it might be that other processes take place at lower potentials (further from the onset potential), possibly related to the formation of a second, less active species as previous observations (Figure 5.1) did show the existence of a second species after reduction. Also, the complex might also be more prone to degradation at lower potentials.

5.3 Discussion

As demonstrated, EWG's and a EDG can alter the electrochemical and electrocatalytic properties of **1**. First of all, the $E_{1/2}$ of redox the couple had an expected Hammett correlation with the different substituents used in this study. In contrast, the O_2 reduction onset potential was not influenced by electronic character of the substituents. This observation points to an O_2 reduction mechanism wherein the potential determining step is not related to the $E_{1/2}$ of the complex. On the other hand, a slight performance boost for $\mathbf{2^{Cl}}$ with respect to **1** was found. Based on these findings, we suggest that the apparent (observed) mechanism is not best described by Equations 5.1 and 5.2. Based on the immensely fast O_2 reduction by **1**, that can achieve 10^5 turnovers of O_2 per second at micromolar catalyst concentrations,[10] we argue that that the observed potential determining step first is not the 1 electron reduction of the Cu^{II} to the Cu^{I} complex step (Eqn. 5.1), but rather related to the simultaneous coordination of O_2 and reduction to a superoxo species according to Equation 5.4. The reduction of the Cu^{II} complex (Eqn. 5.1) and the subsequent coordination of O_2 resulting in the superoxo species (Eqn. 5.2) are both very fast and can be considered instantaneous on the time scale of the cyclic voltammograms with scan rates of 50 or 100 mV/s. For that reason, the reduced Cu^{I} complex might be seen as a transient species and not as an intermediate (Eqn. 5.5). Following, the

overall equilibrium of Equation 5.5 could be covered by Equation 5.6 with a separate $E_{1/2}$'.

$k_1'/E_{1/2}'$ $\quad Cu^{II} + O_2 + e^- \rightleftharpoons Cu^{II}O_2^{\bullet -}$ **Eqn. 5.4**

k_1 / k_2 $\quad Cu^{II} + e^- \overset{k_1(ET)}{\rightleftharpoons} \left[Cu^{I}\right] \overset{k_2(O_2)}{\rightleftharpoons} Cu^{II}O_2^{\bullet -}$ **Eqn. 5.5**

$E_{1/2}'$ $\quad K_{eq}^{\circ} = \dfrac{Cu^{II}}{Cu^{II}O_2^{\bullet -}}$ **Eqn. 5.6**

The potential determining step described by Equation 5.4 suggests that the transferred electron ends up in an orbital on the superoxide moiety which is in a remote position and barely influenced by the ligand. Therefore, there is a minimal effect of ligand substitution on the thermodynamic $E_{1/2}$'. The rate constant of this reaction (k_1') could be related to O_2 coordination and thus still be influenced by the electronic effects of the substituent. In this case, filled orbitals of the O_2 moiety have an interaction (overlap) with orbitals of the copper complex to establish the σ-bonds and π-bonding between the complex and O_2 which involves molecular orbitals that can be influenced by the ligand. Remarkably, $\mathbf{2^{Cl}}$ has a higher O_2 reduction rate, as was found by both the non-rotating electrode and Tafel analysis. On the other hand, the reduction rate of O_2 by $\mathbf{2^{CF3}}$ did not improve significantly. This seems to point to an additional effect of the chloride substituents apart from having an electron withdrawing character that does not directly correlate to the Hammett parameter. Examples of correlations between the (electro)catalytic rate and the Hammett parameter are known and will be discussed later. Of note, the Hammett parameter is based on substitution reactions of aromatic C–H bonds. In the case of O_2 coordination and further reduction to H_2O_2, processes such as π-backbonding play an important role. A p-orbital of the chloride substituent can conjugate with the orbitals of the pyridine ring, thereby changing the energy of the pyridinic orbitals via delocalization. Perhaps, this results in better overlap of the orbitals involved in O_2 coordination to facilitate π-backbonding. These processes are more complicated and may not be fully captured in the magnitude of the Hammett parameter and could explain why the reactivity of $\mathbf{2^{Cl}}$ is different from **1** and $\mathbf{2^{CF3}}$. Apart from the suggested potential and rate determining step linked in Eqn. 5.4, another possibility would be that the potential and rate determining step are related to the step of Equation 5.3. However, we argue that the proton coupled electron transfer involving

$Cu^{II}–O_2^{\bullet-}$ would not be the limiting step in the presence of water and the high concentration (0.1 M) of phosphate buffer.

Applying a FOWA to a catalytic reaction with Equation 5.4 as (observed) potential determining step is problematic. To be able to use the FOWA to calculate the TOF_{max}, the $E_{1/2}$ of the potential determining step is required. In this case for O_2 reduction, that would be the $E_{1/2}$' of Eqn. 5.4. However, this $E_{1/2}$' cannot be determined in aqueous solutions since the $Cu^{II}–O_2^{\bullet-}$ species would directly react further because of the presence of protons. As our results show, the $E_{1/2}$ of the complexes differ due to the substituents. In this particular case, where the TOF_{max} can be in the order of 10^6 s^{-1}, as is the case for **1**,[10] a 100 mV shift of the $E_{1/2}$ that is used can in- or decrease the TOF_{max} by 3 orders of magnitude. Therefore, the $E_{1/2}$ of the complexes cannot be used since these would easily lead to over- or underestimation of the TOF_{max}. Interestingly, the order of magnitude (10^6) of the TOF_{max} for O_2 to H_2O_2 reduction as was determined with the FOWA for **1** was actually close to the actual k_{obs} at low catalyst concentrations determined with the current enhancement method.[10] As these values are in good agreement, the FOWA did not over- or underestimate the TOF_{max} to a large extent, even though the $E_{1/2}$ of **1** was used for the calculation. This indicates that the $E_{1/2}$ of **1** must be close to the $E_{1/2}$' of Eqn. 5.4. The k_1' of the complexes is most likely in the order of $\mathbf{2^{Cl}} > \mathbf{1} \approx \mathbf{2^{CF3}} > \mathbf{3^{NH2}}$.

The mechanism for H_2O_2 reduction has been less well explored. Our results show that the electronic effect of the EWG's of $\mathbf{2^{Cl}}$ and $\mathbf{2^{CF3}}$ have shifted the onset positively and significantly improved the rate according to the Tafel analysis. The exact mechanism is unknown, but could be Fenton type chemistry in which H_2O_2 is split in a copper bound hydroxyl ($Cu^{II}–OH$) and free hydroxyl radical ($OH^{\bullet-}$).[26, 27] Another possibility would be a mechanism wherein a copper–oxyl species ($Cu^{II}–O^{\bullet}$) is formed, as is proposed for the *modus operandi* of lytic polysaccharide monooxygenases (LPMO). In the LPMO mechanism, derived from computational research, the O–O bond of H_2O_2 is first split into a copper bound hydroxyl and a hydroxyl radical.[28] In contrast to Fenton type chemistry, the free hydroxyl radical immediately abstracts a hydrogen atom from the copper–hydroxyl species giving rise to a $Cu^{II}–O^{\bullet}$ radical species. The unique hydrogen bonding framework within the enzyme stabilizes this Cu^{II} oxyl radical so that it exclusively oxidizes a substrate instead of causing damage to the amino acid residues that surround the active site. Moreover, this mechanism ensures that the highly reactive free hydroxyl radical is quickly "trapped" to avoid damage. Copper–oxyl species have been proposed as part of H_2O_2 reduction mechanism, though direct evidence for the participation of this species remains elusive.[29] The inductive electron withdrawing effect of the EWG's

used in our study could be important to accommodate the negative charge accompanying the formation of the hydroxyl coordinated copper or copper–oxyl species. The higher rate and onset potential of $\mathbf{2}^{\mathbf{Cl}}$ and $\mathbf{2}^{\mathbf{CF3}}$ with respect to **1** is supportive of this theory.

The most remarkable outcome of our study is that influence of the substituents on the onset potential and the catalytic rate differs for O_2 reduction and H_2O_2 reduction. While for O_2 reduction the onset potential was not influenced by EWG's, the onset potential and catalytic rate both increased for H_2O_2 reduction. Nevertheless, correlations between substituted complexes and the corresponding catalytic parameters have been shown to differ significantly depending on the studied system. Generally, the $E_{1/2}$ of the complexes is considered as reference for the electron density around the metal center and its influence on the onset potential and catalytic rate. A typical finding in most cases is that a higher onset potential, induced by substituents or differences in geometry, decreases the catalytic rate in electrocatalytic reductions such as O_2,[30] H_2,[31, 32] and CO_2[33] reduction. For example, the electrochemical O_2 and H_2O_2 reduction by bipyridine or terpyridine chelated copper complexes displays inverse linear relationships between the $E_{1/2}$ and the reduction rate.[34] The higher the $E_{1/2}$, the lower the rate. EWG's on these terpyridine or bipyridine ligands directly increased the $E_{1/2}$,[30] which is in agreement with our findings. In rare cases, a different effect was found. One example includes mononuclear ruthenium water oxidation catalysts for which the $E_{1/2}$ was found to increase with EDG's instead of EWG's. Moreover, the $E_{1/2}$ correlated with the Hammett parameter of the substituents.[35] This remarkable effect was explained by the pK_a of the uncoordinated imidazole moiety of the ligand. That pK_a changed upon substitution and had an overall dominant electronic effect on the $E_{1/2}$ when protonated or deprotonated. Nevertheless, no clear linear correlation between the Hammett parameters ($E_{1/2}$ of the complexes) and the rate of water oxidation was found. It was suggested that EDG's changed the mechanism of water oxidation and thus the rate determining step. The found relationships were therefore not linear but rather a polynomial function. Another aspect to consider, is that the $E_{1/2}$ is not always a direct indication of the electronic nature of the ligand and its influence on the activity. For example, the $E_{1/2}$ of pyridyl alkylamine copper complexes like **1** can be shifted by changing the linker length between the central amine and the pendant pyridine or by substituting a chelating pyridine with a non-chelating benzene arm.[36] In that case, the major influence of the ligand is on the geometry of the resulting complex which in turn affects the $E_{1/2}$ as opposed to electronic effects induced by substituents. However, there was no clear link between the $E_{1/2}$ and the O_2 reduction

activity. Differences in steric hindrance as a result of these diverse geometries could significantly affect the mechanism and even change, for example, the interaction with H_2O_2 from mononuclear to dinuclear.[37] A combination of a higher $E_{1/2}$ and faster catalysis, as we found for H_2O_2 reduction by $\mathbf{2^{Cl}}$ and $\mathbf{2^{CF3}}$ as compared to **1**, is not unique. A series of substituted nickel bis(diphosphine) based electrocatalysts for H_2 reduction showed a similar correlation.[38] In that study, complexes with EWG's had increased H_2 reduction activity while the overpotential decreased as well. In another study that investigated a range of manganese based substituted phthalocyanine complexes, the redox couple of a part of the investigated complexes had a direct linear correlation with the catalytic current, though a small part of the complexes deviated significantly from the fits.[39] Another example is the electrocatalytic CO_2 reduction by iron porphyrins which was improved by EWG's on the porphyrin that increased the rate of catalysis and reduced the required overpotential.[40] In general, correlations between the $E_{1/2}$ of the complex, the catalytic rate, and catalytic onset potential are found. Often, EWG's increase the $E_{1/2,}$ can reduce the onset potential (of a reduction), but decrease the catalytic rate. Nevertheless, the mentioned studies clearly show that exceptions to these rules are found frequently. In these cases, the Hammett parameter is too simplistic to fully explain the electron density of the metal active site. Furthermore, secondary effects such as geometry and steric hindrance can significantly influence the $E_{1/2}$ but do not immediately correlate to the catalytic activity. It is therefore not unique that our catalytic results for both O_2 and H_2O_2 reduction by the substituted complexes based on **1** deviate from general expectations due to, for instance, the previously mentioned influence of π-backbonding.

5.4 Conclusion

The electronic influence of electron withdrawing and electron donating groups on **1** have been investigated for both the electrochemical O_2 and H_2O_2 reduction. The Hammett parameter of the substituents correlates directly with the thermodynamic redox potential ($E_{1/2}$) of the $Cu^{I/II}$ redox couple. However, the onset potential for O_2 reduction is not affected. We believe that the observed O_2 to H_2O_2 reduction mechanism does not have a potential determining step related to the $E_{1/2}$ of the complex, but rather to the thermodynamic equilibrium potential of an apparent simultaneous reduction and O_2 coordination of the Cu^{II} complex (Eqn. 5.4) due to the very fast kinetics of O_2 coordination to the copper complexes. The implication of this mechanism would be that the onset potential of O_2 reduction by **1** cannot be

improved by electronic effects of substituents as was found in this study. However, the rate of catalysis was slightly improved as a result of placing a chloride group on the *para* position of the pyridines of **1**. Interestingly, the CF_3 group, that is also a EWG and has a higher Hammett parameter than Cl, did not improve the catalytic rate with respect to the unsubstituted complex. The reason for this could be the ability of electron delocalization properties of Cl with the pyridine moiety that influences the π-backbonding with O_2. In contrast, H_2O_2 reduction by the EWG's substituted complexes clearly started at a higher potential than the unsubstituted complex. Remarkably, the rate of reduction improved as well. There is a better correlation of the H_2O_2 reduction rate to the Hammett parameter as compared to the correlation to the O_2 reduction rate. Nevertheless, the reactivity of **1** is lower than expected for H_2O_2 reduction whereas chloride substitution resulted in the highest catalytic rate again. Once more, delocalization could play a role in stabilizing the transition state of the rate determining step, but requires more studies since the H_2O_2 reduction mechanism is well understood. Overall, we have shown that by placing EWG groups we have significantly improved the onset potential and catalytic rate of the electrochemical H_2O_2 to H_2O reduction.

5.5 Acknowledgements

Austin Herzog is kindly acknowledged for the synthesis of $\mathbf{2}^{Cl}$ and $\mathbf{2}^{CF3}$. Michiel Langerman is thanked for supplying a sample of **1**. Professor Kenneth Karlin is acknowledged for the collaboration on this project. This work has been financially supported by the European Research Council (ERC starting grant 637556 Cu4Energy to dr. D.G.H. Hetterscheid) and the Leiden Institute of Chemistry.

5.6 Experimental

5.6.1 General

All chemicals that have been used for synthesis and electrochemistry were purchased from commercial suppliers and used as received, unless mentioned otherwise. The complexes $\mathbf{2}^{CF3}$ and $\mathbf{2}^{Cl}$ were synthesized by Austin Herzog from the Karlin group at the John Hopkins University from Baltimore, the United States of America and used as received. Nuclear magnetic resonance (NMR) measurements were performed on a Bruker DPX 300 spectrometer. UV-vis measurements were performed on a Varian Cary UV-vis spectrometer. Mass spectra were obtained on a Thermo Fisher Scientific MSQ Plus ESI. High resolution mass spectra (HR MS) were

obtained on a Thermo Finnigan LTQ Orbitrap. Calibration was performed with a calibration mixture obtained from Thermo Finnigan prior to the measurement. Elemental analysis was performed by Mikroanalytisch Laboratorium Kolbe from Oberhausen, Germany. For pH measurements, a Hannah instruments HI 4222 pH meter was used and calibrated with five different IUPAC standard buffers.

5.6.2 Synthesis

Synthesis of 2-hydroxymethyl-4-nitropyridine (4)

The synthesis was based on a previously reported synthesis.[41] 10.5 g of 4-nitro-2-picoline-N-oxide (Fluorochem) was dissolved in 100 ml dichloromethane (DCM, Honeywell). Over the course of 20 minutes, 22.5 ml trifluoroacetic anhydride (Alfa Aesar) in 25 ml DCM was added dropwise. The mixture turned yellow to red. When finished, the mixture was refluxed for 18 h (overnight). Next, the mixture was concentrated under reduced pressure. 100 ml demineralized water was added. Subsequently, K_2CO_3 was carefully added while stirring until the pH was 8. The mixture was left to stir for 1 hour while the color turned yellow again. The pH was checked, additional K_2CO_3 was added and the mixture was left to stir for 5 more hours. Next, 10 M NaOH was added to raise the pH to circa 10-12 and the mixture was stirred for 30 minutes after which DCM was added. The layers of the mixture were separated subsequently and the aqueous layer was extracted twice with DCM. All organic layers were collected and dried over Na_2SO_4 before being filtered. All volatiles were removed under reduced pressure. A yellow oil was obtained which slowly crystallized into a yellow solid. After column chromatography on silica with 3:1 Et_2O:PetEt as eluent, 2.50 gram of a slightly yellow solid was obtained (16.2 mmol, 25%). ^{1}H NMR matched the values reported in literature of **4** within 0.04 ppm (apart from the hydroxyl, for which the shift depends heavily on the acidity of the solvent).[41]

ESI MS *m/z* (found (calculated)): 155.2 (155.1 [M + H^+]). ^{1}H NMR (300 MHz, $CDCl_3$) δ 8.83 (d, 1H, ^3J(H,H) = 5.4 Hz, *m*-(NO_2-Py)-*H*), 8.09 (m, 1H, *m*-$HOCH_2$-(NO_2-Py)-*H*), 7.92 (dd, 1H ^3J(H,H) = 5.5 Hz, ^4J(H,H) = 2.1 Hz, *m*-(NO_2-Py)-*H*), 4.91 (s, 2H, HOCH_2-(NO_2-Py)), 3.79 (s, 1H, *H*OCH_2-(NO_2-Py)).

Synthesis of 2-chloromethyl-4-nitropyridine (5)

Compound **5** was prepared by following a procedure for the conversion of a 4-chloro anologue.[18] 2.51 g of 2-hydroxymethyl-4-nitropyridine (**4**) was dissolved in 80 ml DCM. Next, 2 ml $SOCl_2$ was added slowly over the course of 2 minutes. A

precipitation formed. The mixture was stirred at room temperature and followed by TLC. After 20 h, saturated $NaHCO_3$ solution was added to quench the reaction while stirring vigorously until the mixture reached neutral pH. The organic layer was separated and the aqueous layer was extracted 3 times with DCM. All organic fractions were combined and dried over Na_2SO_4. Volatiles were removed under reduced pressure after filtration. A yellow oil was obtained. This was dissolved in a minimum amount of a 3:1 mixture of pentane:Et_2O and a few drops of DCM. This was loaded on a silica (Screening Devices, Silica Gel 40-63 μm) column and the product was obtained with 3:1 pentane:Et_2O as eluent. All product fractions were combined and the volatiles were removed under reduced pressure. 2.30 g of yellow oil was obtained (14.9 mmol, 92%). The purity was assessed by TLC and based on experience of the preparation of a smaller batch. No further characterization was performed since the product is very unstable when it is not dissolved. Directly after the yield was determined, the product was immediately used in the next reaction. As said, a smaller batch was prepared and the purity of that batch was assessed by ^{1}H NMR. The spectra matched literature values within 0.03 ppm.[42] ^{1}H NMR (300 MHz, $CDCl_3$) δ 8.87 (dd, 1H, ^3J(H,H) = 5.4 Hz, ^5J(H,H) = 0.6 Hz, *o*-(NO_2-Py)-*H*), 8.23 (dd, 1H, ^4J(H,H) = 2.1 Hz, ^5J(H,H) = 0.6 Hz, *m*-$ClCH_2$-(NO_2-Py)-*H*), 7.98 (dd, 1H, ^3J(H,H) = 5.4, ^4J(H,H) = 2.1 Hz, *m*-(NO_2-Py)-*H*), 4.79 (s, 2H, Cl*H*$_2$-(NO_2-Py)).

Synthesis of bis[(4-nitro-2-pyridyl)methyl]-2-pyridylmethyl-amine (6)

Directly after the purification of 2-chloromethyl-4-nitropyridine (compound **5**) by column chromatography in the previous step, 2.3 g of the compound was directly dissolved in 30 ml MeCN (dried over molecular sieves, purged with N_2, Biosolve HPLC grade) under N_2 atmosphere. Next, 654 μL 2-picolylamine (Sigma Aldrich) was dissolved in 20 ml dry MeCN and transferred to the mixture. The mixture became darker yellow. Next, 3.3 ml diisopropylethylamine (DIPEA, Acros) and 95 mg KI (Sigma Aldrich) were added and the mixture was heated at 60 °C. The mixture became dark brown over time. The reaction was followed over time by TLC on alumina with dichloromethane + 2% MeOH as eluent. After 1 day, the reaction was stopped and saturated $NaHCO_3$ solution, water, and ethyl acetate were added. The layers were separated. The aqueous layer was extracted 4 times with ethyl acetate. All organic layers were combined and dried over Na_2SO_4. After filtration, volatiles were removed under reduced pressure. A thick brown oil was obtained. Purification was performed with alumina column chromatography (Brockmann Type 1). A gradient eluent was used starting with DCM. The product was collected by switching the eluent to 0.4% methanol in DCM. Most product was collected in a pure

fraction: 1.35 g (3.55 mmol) but a second round of column chromatography of a collected mixed fraction increased the yield of the thick brown oil to a total of 1.635 g (4.3 mmol, 68%).

HRMS *m/z* (found (calculated)): 381.13026 (381.13058, [M + H^+]), 403.11209 (403.11252, [M + Na^+]). ^{1}H NMR (300 MHz, $CDCl_3$) δ 8.84 (d, 2H, ^3J(H,H) = 5.4 Hz, *o*-(NO_2-Py)-*H*), 8.57 (ddd, 1H ^3J(H,H) = 4.8 Hz, ^4J(H,H) = 1.7 Hz, ^5J(H,H) = 0.9 Hz, *o*-Py-*H*), 8.31 (d, 2H, ^4J(H,H) = 1.9 Hz, *m*-NCH_2(NO_2-Py)-*H*), 7.87 (dd, 2H, ^3J(H,H) = 5.4 Hz, ^4J(H,H) = 2.2 Hz, *m*-(NO_2-Py)-*H*), 7.69 (td, 1H, ^3J(H,H) = 7.7 Hz, ^4J(H,H) = 1.8 Hz, *p*-Py-*H*), 7.49 (dt, 1H, ^3J(H,H) = 7.8 Hz, $^{4,5}J$(H,H) = 1.2 Hz *m*-NCH_2Py-*H*), 7.18 (ddd, 1H, ^3J(H,H) = 7.4 Hz, ^3J(H,H) = 4.9, ^4J(H,H) = 1.1 Hz, *m*-Py-*H*), 4.11 (s, 4H NC*H*$_2$(NO_2-Py)), 3.97 (s, 2H, NC*H*$_2$Py). ^{13}C NMR (75 MHz, $CDCl_3$) δ 163.07 (NCH_2*C*-(NO_2-Py)), 158.18 (NCH_2*C*-Py), 154.60 (O_2N-*C*-Py), 151.55 (*o*-(NO_2-Py)-*C*H), 149.59 (*o*-Py-*C*H), 136.85 (*p*-Py-*C*H), 123.35 (*m*-NCH_2Py-*C*H), 122.63 (*m*-Py-*C*H), 115.72 (*m*-NCH_2-(NO_2-Py)-*C*H), 114.83 (*m*-(NO_2-Py)-*C*H), 60.71 (N*C*H_2-Py), 60.00 (N*C*H_2-(NO_2-Py)). See Appendix D Figures D.7 to D.11 for the ^{1}H NMR, ^{13}C APT, COSY, HSQC, and HMBC NMR spectra.

5

Synthesis of bis[(4-amino-2-pyridyl)methyl]-2-pyridylmethyl-amine (7)

To synthesize **7**, the nitro groups of **6** were catalytically reduced by Pd/C with hydrazine as reducing agent. Of note, other reducing agents did not yield the product. H_2 does not react while $NaBH_4$ leads to a mixture of azo compounds. These latter compounds can be further reduced to amines and the desired product with hydrazine. However, it is best to start with Pd/C and hydrazine from start to avoid the formation of by-products. 0.285 g of **6** was dissolved in 15 ml EtOH (Honeywell). Next, 134 mg Pd/C (10%, Sigma Aldrich) was added and rinsed of the sides of the flask with 15 ml extra EtOH. The mixture was stirred and purged with N_2 for 1 hours. Next, 3 ml hydrazine hydrate (80%, Sigma Aldrich) was added dropwise and the mixture was heated at 60 ° C under N_2 atmosphere. The reaction was followed by thin layer chromatography (TLC) on alumina with $CHCl_3$ with 20% methanol and 1% triethylamine as eluent. Full conversion was obtained after 1 day. The mixture was filtered over celite and washed copiously with EtOH. The filtrate was concentrated under reduced pressure. When *circa* 5 ml remained, water and $CHCl_3$ were added and mixed thoroughly. Subsequently, the layers were separated. The aqueous layer was extracted 3 times with $CHCl_3$. All organic layers were combined, dried over Na_2SO_4 and filtered. All volatiles were removed under reduced pressure. The remaining pale yellow oil was dried under reduced pressure. Over time, the oil solidified. 131 mg (0.408 mmol, 54%) of **7** was obtained.

ESI MS *m/z* (found (calculated)): 321.2 (321.2 [M + H^+]); 343.2 (343.2 [M + Na^+]); 290.3 (290.15, [M + 2 H^+]). ^{1}H NMR (300 MHz, MeOD) δ 8.43 (ddd, 1H, ^3J(H,H) = 5.0 Hz, ^4J(H,H) = 1.8 Hz, ^5J(H,H) = 1.0 Hz, *o*-Py-*H*), 7.89 (dd, 2H, ^3J(H,H) = 5.9 Hz, ^5J(H,H) = 0.5 Hz, *o*-(NH_2-Py)-*H*), 7.80 (td, 1H, ^3J(H,H) = 7.8 Hz, ^4J(H,H) = 1.8 Hz, *p*-Py-*H*), 7.67 (dt, 1H, ^3J(H,H) = 7.8 Hz, $^{4,5}J$(H,H) = 1.1 Hz, *m*-NCH_2Py-*H*), 7.28 (ddd, 1H, ^3J(H,H) = 7.5 Hz, ^3J(H,H) = 5.0 Hz, ^4J(H,H) = 1.3 Hz, *m*-Py-*H*), 6.82 (d, 2H, ^4J(H,H) = 2.3 Hz, *m*-NCH_2(NH_2-Py)-*H*), 6.46 (dd, 2H ^3J(H,H) = 5.9 Hz, ^4J(H,H) = 2.4 Hz, *m*-(NH_2-Py)-*H*), 3.79 (s, 2H, NC*H*$_2$Py), 3.64 (s, 4H, NC*H*$_2$(NH_2-Py)),). Signals corresponding to the NH_2 protons were not observed possibly due to fast exchange with deuterium from the solvent. ^{13}C NMR (75 MHz, MeOD) δ 160.25 (H2N*C*-(NH_2-Py)), 159.04 (*o*-NCH_2*C*-Py), 157.75 (*o*-NCH_2*C*-(NH_2Py)), 149.39 (*o*-Py*C*H), 148.52 (*o*-(NH_2-Py)*C*H), 138.69 (*p*-Py*C*H), 124.90 (*m*-NCH_2Py*C*H), 123.85 (*m*-Py*C*H), 109.20 (*m*-NCH_2(NH_2-Py)*C*H), 109.15 (*m*-(NH_2-Py)*C*H), 60.91 (N*C*H$_2$Py), 60.58 (N*C*H$_2$(NH_2-Py)). See Appendix D Figures D.12 to D.16 for the ^{1}H NMR, ^{13}C APT, COSY, HSQC, and HMBC NMR spectra.

5

Synthesis of [Cu(2NO_2-tmpa)(CH_3CN)](CF_3SO_3)$_2$ (3^{NO2})

108 mg **6** and 99 mg Cu(OTf)$_2$ were dissolved in 10 ml MeOH and stirred for 2 hours at room temperature. Next, all volatiles were removed under reduced pressure. The turquoise colored oil was washed with hexane 3 times and 2 times with Et_2O. Next, hexane was added and all volatiles were removed under reduced pressure. The last step was repeated 3 times. Small crystals appeared. Next, the crude solid/oil was dissolved in a minimum amount of MeCN. Vapor diffusion with Et_2O at 5 °C resulted in the formation of blue crystals. After filtration, the crystals were washed with a 1:9 MeCN:Et_2O mixture. After drying the crystals under reduced pressure, 85.9 mg of crystals (0.112 mmol, 41%) was obtained.

Elemental analysis calculated ratio (%) for [Cu((**6**)(CH_3CN)](OTf)$_2$ ($C_{22}H_{19}CuF_6N_7O_9S_2$)+ 1.6 H_2O: C 33.20, H 2.81, N 12.32; found: C 33.01, H 2.63, N 12.21. UV-vis λ_{max}: 285 nm, 690 nm, 890 nm (0.3 mM in pH 7 phosphate buffer, Figure D.2).

5.6.3 General electrochemistry

For the preparation of buffers, the cleaning of glassware, cleaning of the electrodes, Milli-Q grade Ultrapure water (>18.2 MΩ cm resistivity) was used. A 0.1 M phosphate buffer of pH 7 was used. This buffer was prepared from NaH_2PO_4 (Merck Suprapur ©, 99.99%) and Na_2HPO_4 (Fluka Traceselect© 99.995%). The electrolyte was purged with Ar (Linde, Ar 5.0) for 30 minutes or O_2 (Linde, O_2 5.0)

for 20 minutes prior to the experiment. During measurements, a constant flow of O_2 or Ar was kept above the solution. For H_2O_2 reduction measurements, H_2O_2 for ultratrace analysis (Sigma Aldrich) was used and diluted with Milli-Q water. For RRDE measurements, the electrolyte was purged during the measurement as well. Electrochemical measurements were performed in custom-made, single compartment glass cells. For RRDE, a different cell was used that will be described in a separate section. All glassware was cleaned by boiling in water and extensive rinsing prior to each experiment. Periodically, the glassware was cleaned by immersing it in a 1 g/L $KMnO_4$ (Sigma) solution in 0.5 M H_2SO_4 (Sigma, reagent grade) for at least a night. Next, the glassware was extensively rinsed with water and immersed in water with a few drops of concentrated H_2SO_4 and H_2O_2 (Merck Emprove 35%). After all MnO_2 residues had been oxidized, the glassware was rinsed and boiled in water for 3 consecutive times. Prior to each RRDE measurement, this extensive cleaning procedure was performed. A three electrode setup with Autolab PGSTAT 12 and 204 and IVIUM CompactStat potentiostats were used. NOVA 2.1 or IVIUM software were used.

For all measurements, a reversible hydrogen electrode (RHE) was used as reference electrode. This was either a HydroFlex (Gaskatel) or a Platinum mesh in H_2 (Linde, H_2 5.0) saturated electrolyte operating at the same pH as the working electrode and connected to the cell via a Luggin capillary. In all cases, the counter electrode was a large surface area gold wire that was flame annealed prior to each measurement. The working electrode (not for RRDE), was a glassy carbon (GC) electrode (0.07 cm^2, Metrohm) encapsulated in polyether ether ketone (PEEK). Before each measurement, the electrode was mechanically polished. When extensive polish was required, P2500 sand paper was used for 10 seconds before the usual polishing procedure. For the regular polish, a Labopol 20 polishing machine with 1.0 micron diamond and 0.04 micron silica suspension on Dur-type polishing cloths were used (all from Struers). The GC was polished for 1 minute after which it was rinsed with water and isopropanol (after the diamond slurry) or water only (after the silica suspension). Next, the electrode was sonicated in water for 10 minutes and rinsed copiously with water. Before each measurement, the quality of the polish was checked by running a CV in catalyst-free electrolyte under O_2 and/or Ar.

5.6.4 RRDE

Rotating ring disk electrode experiments were performed in a custom-made glass cell with three different compartments for the reference, counter and work electrode. Water permeable glass frits were used to separate the compartments. The

work electrode was a glassy carbon disk (0.196 cm^2) that was used in a ChangeDisk configuration with a Platinum ring all of which were obtained from Pine. A Pine rotator was used. The GC disk was polished as described before and separately from the Pt ring. The Pt ring was polished following the same procedure as glassy carbon. Generally, the setup was rotated at 1600 rpm. For the O_2 and H_2O_2 reduction measurements of $\mathbf{3^{NH_2}}$ a 0.05 M phosphate buffer of pH 7 was used.

5.7 References

1. Gewirth, A. A.; Thorum, M. S., *Inorg. Chem.* **2010,** *49*, 3557–3566.
2. Nørskov, J. K.; Rossmeisl, J.; Logadottir, A.; Lindqvist, L.; Kitchin, J. R.; Bligaard, T.; Jónsson, H., *J. Phys. Chem. B* **2004,** *108*, 17886–17892.
3. Gasteiger, H. A.; Kocha, S. S.; Sompalli, B.; Wagner, F. T., *Appl. Catal., B* **2005,** *56*, 9–35.
4. Campos-Martin, J. M.; Blanco-Brieva, G.; Fierro, J. L. G., *Angew. Chem. Int. Ed.* **2006,** *45*, 6962–6984.
5. Eul, W.; Moeller, A.; Steiner, N., Hydrogen Peroxide. In *Kirk-Othmer Encyclopedia of Chemical Technology* [Online] John Wiley & Sons, Inc.: 2000. http://dx.doi.org/10.1002/0471238961.0825041808051919.a01.pub2.
6. Hage, R.; Lienke, A., *Angew. Chem. Int. Ed.* **2006,** *45*, 206–222.
7. Süss, H. U., Bleaching. In *Ullmann's Encyclopedia of Industrial Chemistry*, 2012.
8. Legrini, O.; Oliveros, E.; Braun, A. M., *Chem. Rev.* **1993,** *93*, 671–698.
9. Metcalf & Eddy Inc.; Tchobangolous, G., *Wastewater Engineering: Treatment and Resource Recovery*. 5th edition ed.; Mcgraw-Hill Education: 2014.
10. Langerman, M.; Hetterscheid, D. G. H., *Angew. Chem. Int. Ed.* **2019,** *58*, 12974–12978.
11. Bratsch, S. G., *J. Phys. Chem. Ref. Data* **1989,** *18*, 1–21.
12. Bullock, R. M.; Appel, A. M.; Helm, M. L., *Chem. Commun.* **2014,** *50*, 3125–3143.
13. Costentin, C.; Drouet, S.; Robert, M.; Savéant, J.-M., *J. Am. Chem. Soc.* **2012,** *134*, 11235–11242.
14. Costentin, C.; Savéant, J.-M., *ChemElectroChem* **2014,** *1*, 1226–1236.
15. Costentin, C.; Savéant, J.-M., *J. Am. Chem. Soc.* **2017,** *139*, 8245–8250.
16. Rountree, E. S.; McCarthy, B. D.; Eisenhart, T. T.; Dempsey, J. L., *Inorg. Chem.* **2014,** *53*, 9983–10002.
17. Fry, H. C.; Scaltrito, D. V.; Karlin, K. D.; Meyer, G. J., *J. Am. Chem. Soc.* **2003,** *125*, 11866–11871.
18. Zhang, C. X.; Kaderli, S.; Costas, M.; Kim, E.-i.; Neuhold, Y.-M.; Karlin, K. D.; Zuberbühler, A. D., *Inorg. Chem.* **2003,** *42*, 1807–1824.
19. Enciso, A. E.; Lorandi, F.; Mehmood, A.; Fantin, M.; Szczepaniak, G.; Janesko, B. G.; Matyjaszewski, K., *Angew. Chem. Int. Ed. n/a*.
20. Thorseth, M. A.; Letko, C. S.; Tse, E. C. M.; Rauchfuss, T. B.; Gewirth, A. A., *Inorg. Chem.* **2013,** *52*, 628–634.
21. Ramsey, B. G.; Walker, F. A., *J. Am. Chem. Soc.* **1974,** *96*, 3314-3316.
22. Hammett, L. P., *J. Am. Chem. Soc.* **1937,** *59*, 96–103.
23. Hansch, C.; Leo, A.; Taft, R. W., *Chem. Rev.* **1991,** *91*, 165–195.
24. Smits, N. W. G.; van Dijk, B.; de Bruin, I.; Groeneveld, S. L. T.; Siegler, M. A.; Hetterscheid, D. G. H., *The Influence of Ligand Denticity and Flexibility on the ORR Behavior of Cu-terpy and Cu-bmpa*. **2020,** *Accepted*.
25. Bard, A. J.; Faulkner, L. R., *Electrochemical Methods: Fundamentals and Applications*. Wiley: New York, 2000.
26. Haber, F.; Weiss, J.; Pope, W. J., *Proc. R. Soc. London, Ser. A* **1934,** *147*, 332–351.
27. Garcia-Bosch, I.; Cowley, R. E.; Díaz, D. E.; Siegler, M. A.; Nam, W.; Solomon, E. I.; Karlin, K. D., *Chem. - Eur. J.* **2016,** *22*, 5133–5137.
28. Wang, B.; Johnston, E. M.; Li, P.; Shaik, S.; Davies, G. J.; Walton, P. H.; Rovira, C., *ACS Catal.* **2018,** *8*, 1346–1351.
29. Shimoyama, Y.; Kojima, T., *Inorg. Chem.* **2019,** *58*, 9517–9542.
30. McCrory, C. C. L.; Ottenwaelder, X.; Stack, T. D. P.; Chidsey, C. E. D., *J. Phys. Chem. A* **2007,** *111*, 12641–12650.
31. Hu, X.; Brunschwig, B. S.; Peters, J. C., *J. Am. Chem. Soc.* **2007,** *129*, 8988–8998.

32. Koca, A.; Özçeşmeci, M.; Hamuryudan, E., *Electroanalysis* **2010,** *22*, 1623–1633.
33. Bernatis, P. R.; Miedaner, A.; Haltiwanger, R. C.; DuBois, D. L., *Organometallics* **1994,** *13*, 4835–4843.
34. Zhang, J.; Anson, F. C., *Electrochim. Acta* **1993,** *38*, 2423–2429.
35. Kärkäs, M. D.; Liao, R.-Z.; Laine, T. M.; Åkermark, T.; Ghanem, S.; Siegbahn, P. E. M.; Åkermark, B., *Catal. Sci. Technol.* **2016,** *6*, 1306–1319.
36. Asahi, M.; Yamazaki, S.-i.; Itoh, S.; Ioroi, T., *Dalton Trans.* **2014,** *43*, 10705–10709.
37. Kunishita, A.; Kubo, M.; Ishimaru, H.; Ogura, T.; Sugimoto, H.; Itoh, S., *Inorg. Chem.* **2008,** *47*, 12032–12039.
38. Kilgore, U. J.; Roberts, J. A. S.; Pool, D. H.; Appel, A. M.; Stewart, M. P.; DuBois, M. R.; Dougherty, W. G.; Kassel, W. S.; Bullock, R. M.; DuBois, D. L., *J. Am. Chem. Soc.* **2011,** *133*, 5861–5872.
39. Sehlotho, N.; Nyokong, T., *J. Electroanal. Chem.* **2006,** *595*, 161–167.
40. Costentin, C.; Robert, M.; Savéant, J.-M., *Acc. Chem. Res.* **2015,** *48*, 2996–3006.
41. Zaman, N.; Guillot, R.; Sénéchal-David, K.; Boillot, M.-L., *Tetrahedron Lett.* **2008,** *49*, 7274–7275.
42. Tamura, M.; Urano, Y.; Kikuchi, K.; Higuchi, T.; Hirobe, M.; Nagano, T., *Chem. Pharm. Bull.* **2000,** *48*, 1514–1518.